The stability analysis of a discrete-time control algorithm for the Canadian advanced nanospace eXperiment-4&5 formation flying nanosatellites

J K Eyer and C J Damaren

Proceedings of the Institution of Mechanical Engineers, Part G: Journal of Aerospace Engineering 2009 223: 441
DOI: 10.1243/09544100JAERO470

The stability analysis of a discrete-time control algorithm for the Canadian advanced nanospace eXperiment-4&5 formation flying nanosatellites

J K Eyer* and **C J Damaren**
University of Toronto Institute for Aerospace Studies, Toronto, Ontario, Canada

The manuscript was received on 17 October 2008 and was accepted after revision for publication on 26 February 2009.

DOI: 10.1243/09544100JAERO470

Abstract: The development of an LQR-based control algorithm for the Canadian advanced nanospace eXperiment (CanX)-4&5 formation flying nanosatellite mission is described. To facilitate an analytical stability proof of the algorithm, elements of the non-linear and continuous system are linearized and discretized. A suitable state for the system is selected and the algorithm is converted into a discrete linear time-varying system that is very nearly periodic. The stability of the system is then determined by means of discrete Floquet theory. This analysis is applied to the CanX-4&5 algorithm during its primary mission of testing along track orbit formations and projected circular orbit formations. The analysis is also applied to the algorithm while executing a quasi J_2-invariant formation. The results in all cases indicate stability. Finally, for the quasi J_2-invariant formation the control authority of the algorithm is reduced until the stability limit is approached and the minimum ΔV required to maintain the formation is found.

Keywords: stability analysis, discrete Floquet theory, linear time-varying system, formation flying satellites, Canadian advanced nanospace eXperiment-4&5

1 INTRODUCTION

The recent paradigm shift towards the use of formation flying in future satellite missions has led to a profusion of research into the dynamics and control problems associated with such systems. Despite rapid progress in the field, however, only a few actual satellite missions are currently under development to either test precision formation flying techniques and solutions or capitalize on the potential benefits of formation flying in real applications. These include the Prototype Research Instruments and Space Mission Technology Advancement mission [**1**], which is a joint project developed by the Swedish Space Corporation and Deutsches Zentrum für Luft- und Raumfahrt; the European Space Agency's (ESA) Proba-3 experiment [**2**]; the Japan Canada Joint Collaboration Satellite–Formation Flying mission from the Japanese Aerospace Exploration Agency and the Canadian Space Agency [**3**]; and ESA's Darwin formation, which will orbit the Earth–Sun L_2 point [**4**].

Given that few fully functional precision formation flying control algorithms have been developed, very little research has focused on the issue of controller stability. Nevertheless, some analytical and numerical stability proofs have been performed on study cases. In reference [**5**] Scheeres and Hsiao design stable control laws to produce bounded relative motion while tracking unstable reference trajectories. In reference [**6**] the authors mathematically define a formation on the basis of control interactions, and then examine the input-to-output stability of the formation with respect to a partitioning of the formation dynamics. Hu and Ng establish a robust formation control method for spacecraft flying with an uncertain dynamics model and then conduct a number of numerical simulations to demonstrate that the relative error is bounded [**7**]. Finally, the authors in reference [**8**] develop a control strategy based on a Lyapunov potential function and then prove its global stability by showing that it satisfies Lyapunov's Theorem.

**Corresponding author: Institute for Aerospace Studies, University of Toronto, 4925 Dufferin St., Toronto, Ontario, M3H 5T6, Canada. email: eyer@utias.utoronto.ca*

An additional formation flying mission is currently under development in the Space Flight Laboratory (SFL) at the University of Toronto Institute for Aerospace Studies. Part of the Canadian Advanced Nanospace eXperiment (CanX) program, the CanX-4&5 mission is a dual-nanosatellite formation flying demonstration mission with the objective of proving that satellite formation flying can be accomplished cheaply, accurately, and autonomously [**9**]. This translates to low mass, rapid development time, and control algorithms which maintain sub-metre tracking accuracy of specific reference trajectories for minimum ΔV requirements. CanX-4&5 are identical 7 kg nanosatellites with a 20 cm cubic form factor.

Over the course of the mission, CanX-4&5 will test a number of familiar formation configurations, including two along track orbit (ATO) formations at relative spacecraft separations of 1000 and 500 m and two projected circular orbit (PCO) formations at separations of 100 and 50 m [**9**]. Following the primary mission and contingent on the amount of remaining fuel, CanX-4&5 will test a low control authority, 'quasi J_2-invariant' formation for long-duration formation flying, the dynamics of which were designed in reference [**10**].

The key challenge of a formation flying satellite mission is to design a control law that will effectively mitigate orbital perturbations for minimum ΔV requirements. CanX-4&5 use a linear state-feedback control law with the gain matrix designed from a discrete-time, linear quadratic regulator (LQR) method. The control accelerations are implemented using pulse width modulation (PWM) with a period of 300 s between each successive thrust. The input to the control law is an error term describing the difference between the 'real' relative state of the satellites and a suitable reference trajectory. The real relative state is a combination of noisy relative position data derived from real-time GPS measurements and noise-free relative velocity estimates generated by an extended Kalman filter (EKF). This helps to accommodate the sensitivity of the LQR controller to noise on velocity measurements. To generate a noiseless, accurate state estimate, the EKF combines noisy – but accurate – GPS state measurements with noise-free inertial state data produced by a low-fidelity onboard propagator every 5 s. A more comprehensive description of the CanX-4&5 control algorithm is presented in section 2.

The stability of this control algorithm is critical to the success of the CanX-4&5 mission. While numerical simulations of the algorithm exhibit stable performance over 50+orbits [**9**], given the novel controller input with relative positions derived from noisy GPS measurements and relative velocities derived from EKF estimations, it would be highly desirable to perform an independent analytical test to verify stability. This article presents such a stability proof for the CanX-4&5 control algorithm.

2 FIONA: THE CANX-4&5 CONTROL ALGORITHM

Both nanosatellites will be equipped with a dedicated onboard computer to run the formation flying algorithm, dubbed Formation Flying Integrated Onboard Nanosatellite Algorithm (FIONA). The principal task of FIONA is to regularly determine the tracking error between a deputy's actual state and its reference trajectory and to compute the optimal thrusts necessary to correct this error. This section discusses the details of the algorithm.

The numerical orbital propagation of spacecraft is most commonly conducted in the geocentric inertial (GCI) reference frame. For two satellites in close formation, $\mathbf{R}_c$ denotes the position of the uncontrolled chief satellite and $\mathbf{R}_d$ the position of the controlled deputy satellite, where $\mathbf{R} = [XYZ]^T$ is the GCI position of a generic satellite and $R = |\mathbf{R}|$ is its orbital radius. The motion of these two satellites will evolve in the GCI frame according to

$$\ddot{\mathbf{R}}_c = -\frac{\mu \mathbf{R}_c}{\mathbf{R}_c^3} + \mathbf{F}(\mathbf{R}_c)_{\text{pert}} \tag{1}$$

$$\ddot{\mathbf{R}}_d = -\frac{\mu \mathbf{R}_d}{\mathbf{R}_d^3} + \mathbf{F}(\mathbf{R}_d)_{\text{pert}} + \boldsymbol{u}_i \tag{2}$$

where μ is the Earth's gravitational constant, $\boldsymbol{u}_i$ is the control force per unit mass in the GCI applied to the deputy during formation flying manoeuvres, and $\mathbf{F}(\mathbf{R})_{\text{pert}}$ is the sum of the orbital perturbation forces acting upon each satellite. In low Earth orbit (LEO), the principal perturbing force is the second zonal harmonic of the Earth's gravitational field, the J_2 effect, expressed in Cartesian coordinates in the GCI as

$$\mathbf{F}(\mathbf{R})_{J_2} = -\frac{3\mu J_2 R_e^2}{2R^7} \begin{bmatrix} X^3 + XY^2 - 4XZ^2 \\ X^2Y + Y^3 - 4YZ^2 \\ 3X^2Z + 3Y^2Z - 2Z^3 \end{bmatrix} \tag{3}$$

where $J_2 = 1.082\,626\,9 \times 10^{-3}$ and R_e is the equatorial radius of the Earth. The higher order terms, J_3 to J_6, have significantly lower influence, but have also been included in all orbital simulations for CanX-4&5. Differential atmospheric drag is another perturbing force in LEO. But since CanX-4&5 will maintain approximately the same ballistic coefficient (i.e. identical attitudes, similar masses), numerical studies have indicated that drag will play a much smaller role than gravitational perturbations. As such, drag models were not included in the FIONA orbital propagator. The dynamics of the two satellites can be written succinctly by representing equations (1) and (2) in state-space form

$$\dot{\mathbf{X}} = \mathbf{F}(\mathbf{X}, t) \tag{4}$$

where $X = [\mathbf{R}_c^T \ \dot{\mathbf{R}}_c^T \ \mathbf{R}_d^T \ \dot{\mathbf{R}}_d^T]^T$. Formation flying control is typically concerned with the relative motion

of the deputy with respect to the chief. This relative motion is best expressed in the Cartesian Hill frame, a local-vertical-local-horizontal reference frame with its origin centred on the chief, its x-axis in the orbit radial direction, its z-axis in the orbit normal direction, and the y-axis completing the right-handed coordinate system. The state of the deputy expressed in the Hill frame is

$$\mathrm{x}(t) = [\mathbf{r}^{\mathrm{T}} \;\; v^{\mathrm{T}}]^{\mathrm{T}} = [x \;\; y \;\; z \;\; \dot{x} \;\; \dot{y} \;\; \dot{z}]^{\mathrm{T}} \tag{5}$$

The relative position, $\mathbf{r}$, can be determined from the inertial position using the expression

$$\mathbf{r} = [x \;\; y \;\; z]^{\mathrm{T}} = \mathbf{C}_{\mathrm{hi}}\delta\mathbf{R} \tag{6}$$

where $\delta\mathbf{R} = [X_{\mathrm{d}} \;\; Y_{\mathrm{d}} \;\; Z_{\mathrm{d}}]^{\mathrm{T}} - [X_{\mathrm{c}} \;\; Y_{\mathrm{c}} \;\; Z_{\mathrm{c}}]^{\mathrm{T}}$ and $\mathbf{C}_{\mathrm{hi}}$ is the rotation matrix from GCI to the Hill frame, given by

$$\mathbf{C}_{\mathrm{hi}}^{\mathrm{T}}(t) = \left[\frac{\mathbf{R}_{\mathrm{c}}}{|\mathbf{R}_{\mathrm{c}}|} \quad \frac{\mathbf{H}_{\mathrm{c}} \times \mathbf{R}_{\mathrm{c}}}{|\mathbf{H}_{\mathrm{c}} \times \mathbf{R}_{\mathrm{c}}|} \quad \frac{\mathbf{H}_{\mathrm{c}}}{|\mathbf{H}_{\mathrm{c}}|}\right] \tag{7}$$

and where $\mathbf{H}_{\mathrm{c}} = \mathbf{R}_{\mathrm{c}} \times \dot{\mathbf{R}}_{\mathrm{c}}$ is the chief's angular momentum per unit mass. The relative velocity of the deputy in the rotating Hill frame can be closely approximated by the expression

$$\boldsymbol{v} = [\dot{x} \;\; \dot{y} \;\; \dot{z}]^{\mathrm{T}} = \mathbf{C}_{\mathrm{hi}}\delta\boldsymbol{V} - \omega^{\times}\mathbf{r} \tag{8}$$

where $\delta\boldsymbol{V} = [\dot{\boldsymbol{X}}_{\mathrm{d}}\, \dot{\boldsymbol{Y}}_{\mathrm{d}}\, \dot{\boldsymbol{Z}}_{\mathrm{d}}]^{\mathrm{T}} - [\dot{\boldsymbol{X}}_{\mathrm{c}}\, \dot{\boldsymbol{Y}}_{\mathrm{c}}\, \dot{\boldsymbol{Z}}_{\mathrm{c}}]^{\mathrm{T}}$, $\omega = [0\,0\,\sqrt{\mu/R^3}]$ is the mean orbital motion of the chief in a circular orbit and where

$$\omega^{\times} = \begin{bmatrix} 0 & -\omega_3 & \omega_2 \\ \omega_3 & 0 & -\omega_1 \\ -\omega_2 & \omega_1 & 0 \end{bmatrix} = \begin{bmatrix} 0 & -\sqrt{\mu/R^3} & 0 \\ \sqrt{\mu/R^3} & 0 & 0 \\ 0 & 0 & 0 \end{bmatrix}$$

Figure 1 illustrates the relationship between the GCI and Hill reference frames.

On orbit, CanX-4&5 will receive GPS measurement updates in the GCI reference frame every 5 s. A GPS signal processing algorithm, provided by the University of Calgary, will provide CanX-4&5 absolute measurements with a GCI position uncertainty of 2–5 m (root mean squared (RMS)) and a GCI velocity uncertainty of 5–10 cm/s (RMS). The algorithm will also produce relative measurements with a Hill position uncertainty of 5–10 cm (RMS) and a Hill velocity of 1–3 cm/s (RMS). Simultaneously, the satellites will be predicting their orbits with an onboard orbital propagator. In simulations of CanX-4&5, however, both the GPS and onboard propagator signals are generated by numerically integrating equations (1) and (2) using a fourth-order Runge–Kutta method with a fixed step of 0.1 s. To approximate the accurate (but noisy) absolute and relative GPS signals from the Calgary algorithm in the CanX-4&5 simulation, the GPS simulated measurements use J_2 through J_6 perturbations

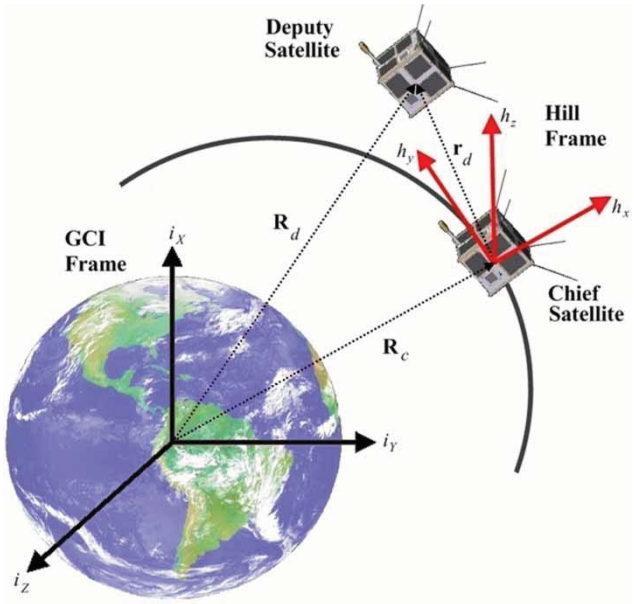

Fig. 1 GCI and Hill reference frames

and normally distributed random Gaussian signals generate the appropriate noise. To represent the lower fidelity but noiseless onboard propagator data, the second propagator uses J_2 perturbations only and has no added noise.

To achieve a single, accurate, and noiseless state estimate, the GPS signal is combined with the onboard propagator signal at each time step using a closed-loop EKF. During the time update phase of the filter at step k, the covariance matrix $\mathbf{P}_k^-$ is generated from the state transition matrix $\boldsymbol{\Phi}_k$ (which, in turn, is developed from the orbital dynamics of equations (1) and (2)) and from the process noise covariance matrix $\mathbf{Q}_k$ [**11**]

$$\mathbf{P}_k^- = \boldsymbol{\Phi}_k\mathbf{P}_{k-1}^+\boldsymbol{\Phi}_k^{\mathrm{T}} + \mathbf{Q}_k \tag{9}$$

During the measurement update phase of the EKF, the GCI state estimate $\hat{\mathbf{X}}_k^+$ is obtained and the error covariance matrix is updated

$$\begin{aligned} \mathbf{K}_k &= \mathbf{P}_k^-\mathbf{H}_k^{\mathrm{T}}(\mathbf{H}_k\mathbf{P}_k^-\mathbf{H}_k^{\mathrm{T}} + \mathbf{R}_k)^{-1} \\ \hat{\mathbf{X}}_k^+ &= \hat{\mathbf{X}}_k^- + \mathbf{K}_k(\mathbf{z}_k - \boldsymbol{h}_k) \\ \mathbf{P}_k^+ &= (1 - K_k\mathbf{H}_k)\mathbf{P}_k^-(1 - K_k\mathbf{H}_k)^{\mathrm{T}} + K_kR_kK_k^{\mathrm{T}} \end{aligned} \tag{10}$$

where $\mathbf{K}_k$ is the Kalman gain matrix, $\mathbf{R}_k$ is the measurement noise covariance, $\mathbf{H}_k$ is the local observation matrix, $\mathbf{z}_k$ is the GPS position measurement, and $\boldsymbol{h}_k$ is the estimated position. The resulting state estimate, $\hat{\mathbf{X}}_k^+$, combines the noiseless characteristics of the onboard propagator with the accuracy of the GPS signal. During GPS lock, the EKF estimated state serves as the input to the onboard propagator for the next

time step, thus maintaining the accuracy of the propagated state. When CanX-4&5 lose contact with the GPS satellites, they enter blackout mode and continue formation flying by simply propagating the last known EKF state until contact with the GPS satellites can be re-established.

During all formation maintenance manoeuvres, FIONA's control law will track a set of pre-established reference trajectories designed to yield periodic relative motion while closely approximating the natural perturbed dynamics of the satellites. Although the actual relative dynamics are non-linear, the Hill–Clohessy–Wiltshire (HCW) equations are linearized approximations of the full dynamics with periodic solutions. They are given in reference [**12**] as

$$\ddot{x} - 2\omega\dot{y} - 3\omega^2 x = 0 \tag{11}$$

$$\ddot{y} - 2\omega\dot{x} = 0 \tag{12}$$

$$\ddot{z} + \omega^2 z = 0 \tag{13}$$

where $\omega = \sqrt{\mu/R^3}$ is the circular orbital rate. By appropriately choosing the constants of integration, the general solutions to the HCW equations can be reduced to the following expressions

$$x_{\text{ref}}(t) = \frac{c_1}{2}\sin(\omega t + \alpha) \tag{14}$$

$$y_{\text{ref}}(t) = c_1 \cos(\omega t + \alpha) + c_3 \tag{15}$$

$$z_{\text{ref}}(t) = c_2 \sin(\omega t + \alpha) \tag{16}$$

where α is the initial formation phase angle and the c_i's are the constants of integration. Selecting $c_1 = c_2 = d_{\text{rel}}$ and $c_3 = 0$, where d_{rel} is the relative spacecraft separation distance, results in a reference trajectory for a PCO of radius d_{rel}. Since the HCW equations assume the chief is in a circular orbit about the Earth, their solutions provide circular reference trajectories for the controller to track in the Hill frame. FIONA employs a linear state-feedback control law to track the reference trajectory

$$\boldsymbol{u}_{\text{h}} = -\mathbf{K}\tilde{\mathbf{x}}, \quad \tilde{\mathbf{x}} = \bar{\mathbf{x}} - \mathbf{x}_{\text{ref}} \tag{17}$$

Here, $\boldsymbol{u}_{\text{h}}$ is the control acceleration in the Hill frame required to correct for the tracking error $\tilde{\mathbf{x}}$. $\mathbf{K}$ is the optimal control gain matrix developed from a discrete-time, LQR method [**9**] and based on a discretization of the linearized HCW dynamics given of equations (11) to (13). In addition, $\mathbf{x}_{\text{ref}}$ is the reference trajectory, represented by equations (14) to (16) for reference positions and their respective derivatives for reference velocities. Under ideal, noiseless conditions $\bar{\mathbf{x}}$ would be the real relative state of the deputy at the current time step, as given by the Calgary GPS processing algorithm. However, as mentioned previously there is an uncertainty associated with the relative GPS measurements: 2–5 cm (RMS) for position and 1–3 cm/s (RMS) for velocity. While the LQR state-feedback controller is robust to noise on the relative position measurements, it is extremely sensitive to noise on the relative velocity data, which leads to unacceptably high ΔV and tracking error penalties. To circumvent this problem, it is necessary to replace the GPS-derived relative velocity measurements with relative velocity data developed from the noiseless inertial state estimate produced by the EKF. The relative position values are still obtained from the processed GPS signals provided by the University of Calgary's algorithm. Consequently, the 'real' relative state input to the controller is defined as

$$\bar{\mathbf{x}} = [x_{\text{GPS}} \;\; y_{\text{GPS}} \;\; z_{\text{GPS}} \;\; \dot{x}_{\text{EKF}} \;\; \dot{y}_{\text{EKF}} \;\; \dot{z}_{\text{EKF}}]^{\text{T}} \tag{18}$$

To implement the control accelerations found by equation (18), the deputy will utilize the Canadian Nanosatellite Propulsion System (CNAPS) [**9**]. Employing liquefied sulphur-hexafluoride as a propellant (with an I_{sp} of ~35 s), CNAPS produces a constant low thrust of 5 mN. Corrective thrusts are therefore implemented discretely via PWM with a period of 300 s (T_{PWM}) between each consecutive thrust. The duration of each thrust can be computed using

$$t_{\text{on}} = \frac{|\boldsymbol{u}_{\text{i}}|}{U_{\max}} T_{\text{PWM}} \tag{19}$$

where $|\boldsymbol{u}_{\text{i}}|$ is the norm of the thrust vector in the inertial frame and $U_{\max}$ is the constant thrust per unit mass of CanX-4&5 ($U_{\max} = 5\,\text{mN}/7\,\text{kg} = 0.0007\,143\,\text{N/kg}$). In addition, the direction of each thrust can be obtained with the expression

$$\boldsymbol{a}_{\text{thrust}} = \frac{u_{\text{i}}}{|u_{\text{i}}|} \tag{20}$$

During each PWM period, FIONA sends the thruster on time, t_{on}, to CNAPS and the attitude target, $\boldsymbol{a}_{\text{thrust}}$, to the attitude control system (ACS) computer. In the simulation of CanX-4&5, the non-impulsive thrusts are fed back into both the GPS and onboard orbital propagators. Figure 2 illustrates the FIONA control algorithm for CanX-4&5. On orbit, the high-fidelity orbital propagator will be replaced by the Calgary GPS algorithm.

3 LINEARIZATION AND DISCRETIZATION OF FIONA

FIONA, as depicted in Fig. 2, is a combination of linear, non-linear, discrete, and continuous elements. Analytically proving the stability of the algorithm in this

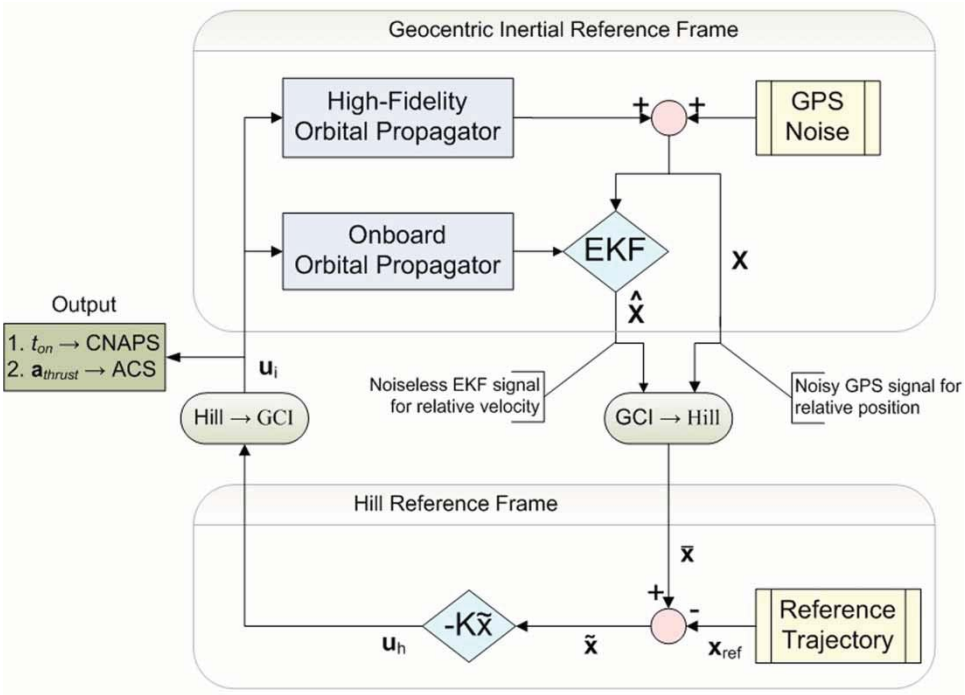

Fig. 2 CanX-4&5 control algorithm, FIONA

form would be very difficult, so to ease the process an approximate model of FIONA must be developed with all elements linearized and discretized. This new model will depend on the state of the chief satellite at each time step, and hence will be a linear time-varying (LTV) system. A discrete LTV system takes the form

$$\boldsymbol{x}_{k+1} = \boldsymbol{\Phi}_k \boldsymbol{x}_k, \quad \boldsymbol{\Phi}_k \in R^{n\times n} \tag{21}$$

where $\boldsymbol{\Phi}_k$ is the state transition matrix between the kth and $(k+1)$th states. The state at an arbitrary time step j is given in reference [**10**] as

$$\boldsymbol{x}_j = \left[\prod_{k=1}^{j} \boldsymbol{\Phi}_{k-1}\right] x_0 \tag{22}$$

where $\boldsymbol{x}_0$ is the initial state. For linear time-invariant systems, where $\boldsymbol{\Phi}_k = \boldsymbol{\Phi}$ is a constant, the most straightforward method of proving global asymptotic stability is to demonstrate that the eigenvalues of $\boldsymbol{\Phi}$ are less than unity. A similar approach can be taken for LTV systems. To develop an appropriate LTV $\boldsymbol{\Phi}_k$ matrix for the CanX-4&5 algorithm, the continuous and non-linear dynamics of the algorithm's orbital propagators need to be linearized and discretized, and the relative dynamics of the HCW equations need to be discretized. Although the discrete LTV system will only be an approximation of the actual algorithm, the short discretization time step of 5 s (corresponding to the GPS data refresh rate) and a linearization about each step will give an accurate representation of the real system.

3.1 Linearization and discretization of the orbital dynamics

The system $\dot{\boldsymbol{x}} = \boldsymbol{f}(\boldsymbol{x})$ with $\boldsymbol{f}(\boldsymbol{x}_0) = 0$ can be linearized by considering a small step $\delta\boldsymbol{x}(t)$ such that $\boldsymbol{x}(t) = \boldsymbol{x}_0 + \delta\boldsymbol{x}(t)$. Then taking a Taylor expansion and retaining only the first-order terms, one obtains

$$\begin{aligned}\dot{\boldsymbol{x}} &= \boldsymbol{f}(\boldsymbol{x}_0 + \delta\boldsymbol{x}) \\ &= \boldsymbol{f}(\boldsymbol{x}_0) + \left.\frac{\partial \boldsymbol{f}}{\partial \boldsymbol{x}^{\mathrm{T}}}\right|_{\boldsymbol{x}=\boldsymbol{x}_k} \delta\boldsymbol{x} + O[\|\delta\boldsymbol{x}\|^2]\end{aligned}$$

Therefore

$$\delta\dot{\boldsymbol{x}} = \left.\frac{\partial \boldsymbol{f}}{\partial \boldsymbol{x}^{\mathrm{T}}}\right|_{\boldsymbol{x}=\boldsymbol{x}_k} \delta\boldsymbol{x} \tag{23}$$

Assuming Keplerian motion (i.e. ignoring non-linear gravitational perturbations which only weakly influence the motion of the deputy), the CanX-4&5 orbital dynamics can be represented for a single satellite as

$$\boldsymbol{f}(\boldsymbol{x}) = [\dot{\mathbf{R}}^{\mathrm{T}} \ \dot{\mathbf{V}}^{\mathrm{T}}]^{\mathrm{T}} \tag{24}$$

Therefore, for one satellite, the matrix of linearized orbital dynamics, $\mathbf{A}$, is the Jacobian of $\boldsymbol{f}(\boldsymbol{x})$ evaluated

at each time step k

$$\mathbf{A} = \left.\frac{\partial \boldsymbol{f}}{\partial \boldsymbol{x}}\right|_{\boldsymbol{x}=\boldsymbol{x}_k} = \left.\begin{bmatrix} \frac{\partial}{\partial \mathbf{R}}(\mathbf{V}) & \frac{\partial}{\partial \mathbf{V}}(\mathbf{V}) \\ \frac{\partial}{\partial \mathbf{R}}\left(\frac{-\mu \mathbf{R}}{R^3}\right) & \frac{\partial}{\partial \mathbf{V}}\left(\frac{-\mu \mathbf{R}}{R^3}\right) \end{bmatrix}\right|_{\mathbf{R}=\mathbf{R}_k}$$

$$= \left.\begin{bmatrix} 0 & 0 & 0 & 1\ 0\ 0 \\ 0 & 0 & 0 & 0\ 1\ 0 \\ 0 & 0 & 0 & 0\ 0\ 1 \\ \frac{\mu}{R^3}\left(\frac{3X^2}{R^2}-1\right) & \frac{3\mu XY}{R^5} & \frac{3\mu XZ}{R^5} & 0\ 0\ 0 \\ \frac{3\mu XY}{R^5} & \frac{\mu}{R^3}\left(\frac{3Y^2}{R^2}-1\right) & \frac{3\mu YZ}{R^5} & 0\ 0\ 0 \\ \frac{3\mu XZ}{R^5} & \frac{3\mu YZ}{R^5} & \frac{\mu}{R^3}\left(\frac{3Z^2}{R^2}-1\right) & 0\ 0\ 0 \end{bmatrix}\right|_{\mathrm{R}=\mathrm{R}_k} \tag{25}$$

For both satellites, the linearized dynamics are $\mathbf{A}_{\mathrm{cd}} = \mathrm{diag}\{\mathbf{A}_{\mathrm{c}}, \mathbf{A}_{\mathrm{d}}\}$. As will be demonstrated in section 6, the gravity terms (i.e. the lower left 3×3 block in equation (25)) can be considered a weak perturbative force and can be ignored without strongly affecting the solution [**13**]. Moreover, for the continuous gain EKF discussed in section 3.3, the gravity terms are also neglected since they are state dependent. The continuous, linear plant to be controlled can be described by a state space model of the form

$$\dot{\mathbf{X}} = \mathbf{A}_{\mathrm{cd}}\mathbf{X} + \mathbf{B}\boldsymbol{u}_{\mathrm{i}} \tag{26}$$

where $\boldsymbol{u}_{\mathrm{i}}$ is the control thrust in the GCI frame and where

$$\mathbf{B} = \begin{bmatrix} 0 & 0 & 0 \\ 0 & 0 & 0 \\ 0 & 0 & 0 \\ 1 & 0 & 0 \\ 0 & 1 & 0 \\ 0 & 0 & 1 \end{bmatrix}$$

Applying a zero-order hold (ZOH) discretization to the continuous orbital dynamics in the GCI frame, $\mathbf{A}_{\mathrm{cd}}$ and $\mathbf{B}$ become

$$\boldsymbol{\Phi}_{\mathrm{i}} = \mathrm{e}^{\mathbf{A}_{\mathrm{cd}}\Delta t} \text{ and } \mathbf{B}_i = \int_0^{\Delta t} \mathrm{e}^{\mathbf{A}_{\mathrm{cd}}\Delta\tau}\,\mathrm{d}\tau\mathbf{B} \tag{27}$$

where Δt is the discretization time step (5 s) and the subscript i indicates the inertial reference frame. The linearized and discretized state-space model becomes

$$\mathbf{X}_{k+1} = \boldsymbol{\Phi}_{\mathrm{i}}\mathbf{X}_k + \mathbf{B}_{\mathrm{i}}\boldsymbol{u}_{\mathrm{i},k} \tag{28}$$

3.2 Discretization of the relative dynamics

The linear HCW dynamics are utilized in the CanX-4&5 algorithm to develop the LQR controller gain, and the solutions of the HCW equations are used as reference trajectories for PCO formation. As will be apparent in section 4, however, the choice of the state for the discrete LTV model requires the relative orbit to be propagated, and it must therefore be discretized. The continuous state-space form of the linear relative model is

$$\dot{\boldsymbol{x}} = \mathbf{A}_{\mathrm{h}}\boldsymbol{x} + \mathbf{B}\boldsymbol{u}_{\mathrm{h}} \tag{29}$$

where

$$\mathbf{A}_{\mathrm{h}} = \begin{bmatrix} 0 & 0 & 0 & 1 & 0 & 0 \\ 0 & 0 & 0 & 0 & 1 & 0 \\ 0 & 0 & 0 & 0 & 0 & 1 \\ 3\omega^2 & 0 & 0 & 0 & 2\omega & 0 \\ 0 & 0 & 0 & -2\omega & 0 & 0 \\ 0 & 0 & -\omega^2 & 0 & 0 & 0 \end{bmatrix},$$

$$\mathbf{B} = \begin{bmatrix} 0 & 0 & 0 \\ 0 & 0 & 0 \\ 0 & 0 & 0 \\ 1 & 0 & 0 \\ 0 & 1 & 0 \\ 0 & 0 & 1 \end{bmatrix}$$

and where the subscript h indicates the Hill reference frame. These continuous dynamics are discretized via a ZOH method, yielding

$$\boldsymbol{\Phi}_{\mathrm{h}} = \mathrm{e}^{\mathbf{A}_{\mathrm{h}}\Delta t} \text{ and } \mathbf{B}_{\mathrm{h}} = \int_0^{\Delta t} \mathrm{e}^{\mathbf{A}_{\mathrm{h}}\Delta\tau}\,\mathrm{d}\tau\mathbf{B} \tag{30}$$

Therefore, the discrete LTV relative model can be written as

$$\boldsymbol{x}_{k+1} = \boldsymbol{\Phi}_{\mathrm{h}}\boldsymbol{x}_k + \mathbf{B}_{\mathrm{h}}\boldsymbol{u}_{\mathrm{h},k} \tag{31}$$

3.3 Constant gain extended Kalman filter

To facilitate the reduction of the CanX-4&5 system in Fig. 2 to a discrete, linearized model, the time-varying EKF was converted to a constant gain EKF (CGEKF). If ($\boldsymbol{\Phi}$, $\mathbf{H}$) is observable and ($\boldsymbol{\Phi}$, $\mathbf{B}$) controllable, the error covariance matrix $\mathbf{P}_k^-$ will converge to a positive definite steady-state (subscript ss) value, $\mathbf{P}_{\mathrm{ss}} > 0$ [**14**], which satisfies the discrete steady-state Riccati equation, given by

$$\boldsymbol{\Phi}\mathbf{P}_{\mathrm{ss}}\boldsymbol{\Phi}^{\mathrm{T}} - \mathbf{P}_{\mathrm{ss}} - \boldsymbol{\Phi}\mathbf{P}_{\mathrm{ss}}\mathbf{H}^{\mathrm{T}}(\mathbf{H}\mathbf{P}_{\mathrm{ss}}\mathbf{H}^{\mathrm{T}} + \mathbf{R})^{-1}\mathbf{H}\mathbf{P}_{\mathrm{ss}}\boldsymbol{\Phi}^{\mathrm{T}} + \mathbf{Q} = 0 \tag{32}$$

As a result, the filter gain will also converge to a steady-state value

$$\mathbf{K}_{\mathrm{ss}} = \mathbf{P}_{\mathrm{ss}}\mathbf{H}^{\mathrm{T}}(\mathbf{H}\mathbf{P}_{\mathrm{ss}}\mathbf{H}^{\mathrm{T}} + \mathbf{R})^{-1} \tag{33}$$

Here $\boldsymbol{\Phi}$ is the discrete GCI orbital dynamics from equation (27), but with the gravity terms neglected.

The metrics used to assess the performance of the CanX-4&5 control algorithm are ΔV (representing fuel expenditure) and tracking error, $\tilde{\boldsymbol{x}}$. Simulations of CanX-4&5 confirm that the CGEKF can replace the time-varying EKF without a loss of accuracy: one orbit in a 1000 m ATO formation yields $\Delta V = 0.059\,18$ m/s and $|\tilde{\boldsymbol{x}}| = 0.2291$ m for both the CGEKF and the EKF.

4 DEVELOPMENT OF THE STATE TRANSITION MATRIX

Choosing an appropriate state vector is a key step to developing a LTV system in the form of equation (21). Since two spacecraft are under consideration, relative states were selected to concisely represent all relevant state information and to reduce the size of the overall state vector. The selected state is

$$\begin{bmatrix} \tilde{\mathbf{x}} \\ \hat{\mathbf{Z}} \end{bmatrix}_k, \text{ where } \tilde{\boldsymbol{x}}_k = \boldsymbol{x}_k - \boldsymbol{x}_{\text{ref},k} \text{ and } \hat{\mathbf{Z}}_k = \hat{\mathbf{X}}_{\text{d},k} - \hat{\mathbf{X}}_{\text{c},k} \tag{34}$$

Here, $\tilde{\mathbf{x}}_k$ is a 6×1 tracking error term between the real relative state of the deputy and the reference trajectory in the Hill reference frame. $\hat{\mathbf{Z}}_k$ is a 6×1 vector difference between the EKF estimates of the deputy's state and the chief's state in the GCI frame. The discrete LTV system can now be reformulated as

$$\begin{bmatrix} \tilde{\mathbf{x}} \\ \hat{\mathbf{Z}} \end{bmatrix}_{k+1} = \begin{bmatrix} \boldsymbol{\Phi}_{11} & \boldsymbol{\Phi}_{12} \\ \boldsymbol{\Phi}_{21} & \boldsymbol{\Phi}_{22} \end{bmatrix}_k \begin{bmatrix} \tilde{\mathbf{x}} \\ \hat{\mathbf{Z}} \end{bmatrix}_k + \begin{bmatrix} \mathbf{B}_1 \\ \mathbf{B}_2 \end{bmatrix}_k \boldsymbol{x}_{\text{ref},k} \tag{35}$$

The remainder of this section is devoted to the determination of the constituent values of $\boldsymbol{\Phi}_k$ and $\mathbf{B}_k$ in equation (35).

4.1 Development of the error state, $\tilde{\mathbf{x}}_{k+1}$

Since the CanX-4&5 algorithm uses relative velocity terms derived from the noiseless EKF estimation for the feedback control law, we can begin by defining this relative state and expressing it in terms of the two states $\tilde{\mathbf{x}}_k$ and $\hat{\mathbf{Z}}_k$

$$\begin{aligned} \bar{\mathbf{x}}_k &= \begin{bmatrix} \mathbf{r} \\ \hat{\mathbf{v}} \end{bmatrix}_k = \begin{bmatrix} \mathbf{r}_\text{d} - \mathbf{r}_\text{c} \\ \hat{\mathbf{v}}_\text{d} - \hat{\mathbf{v}}_\text{c} \end{bmatrix}_k \\ &= \mathbf{M}\bar{\mathbf{C}}_{\text{hi},k}(\mathbf{X}_{\text{d},k} - \mathbf{X}_{\text{c},k}) + \mathbf{N}\bar{\mathbf{C}}_{\text{hi},k}(\hat{\mathbf{X}}_{\text{d},k} - \hat{\mathbf{X}}_{\text{c},k}) \\ &= \mathbf{M}\bar{\mathbf{C}}_{\text{hi},k}\mathbf{Z}_k + \mathbf{N}\bar{\mathbf{C}}_{\text{hi},k}\hat{\mathbf{Z}}_k \end{aligned} \tag{36}$$

Here $\mathbf{M}$ and $\mathbf{N}$ are 6×6 selection matrices designed to isolate position and velocity, respectively. They are defined as

$$\mathbf{M} = \begin{bmatrix} \mathbf{I} & 0 \\ 0 & 0 \end{bmatrix} \quad \text{and} \quad \mathbf{N} = \begin{bmatrix} 0 & 0 \\ 0 & \mathbf{I} \end{bmatrix}$$

Also

$$\bar{\mathbf{C}}_{\text{hi},k} = \begin{bmatrix} \mathbf{C}_\text{hi} & 0 \\ -\boldsymbol{\omega}^\times \mathbf{C}_\text{hi} & \mathbf{C}_\text{hi} \end{bmatrix}_k$$

which depends on the instantaneous state of the chief satellite. As a result, the discrete, linearized system will be timevarying. In equation (36), we must still define $\mathbf{Z}_k$ in terms of $\tilde{\mathbf{x}}_k$ and $\hat{\mathbf{Z}}_k$. If we assume $\mathbf{Z}_k = (\mathbf{X}_{\text{d},k} - \mathbf{X}_{\text{c},k})$, then

$$\tilde{\mathbf{x}}_k = (\boldsymbol{x}_k - \boldsymbol{x}_{\text{ref},k}) = (\bar{\mathbf{C}}_{\text{hi},k}\mathbf{Z}_k - \boldsymbol{x}_{\text{ref},k})$$

Therefore

$$\mathbf{Z}_k = \bar{\mathbf{C}}_{\text{ih},k}\tilde{\mathbf{x}}_k + \bar{\mathbf{C}}_{\text{ih},k}\boldsymbol{x}_{\text{ref},k} \tag{37}$$

where

$$\bar{\mathbf{C}}_{\text{ih},k} = \begin{bmatrix} \mathbf{C}_\text{ih} & 0 \\ \mathbf{C}_\text{ih}\boldsymbol{\omega}^\times & \mathbf{C}_\text{ih} \end{bmatrix}_k$$

The relative state used in the control law now becomes

$$\begin{aligned} \bar{\mathbf{x}}_k &= \mathbf{M}\bar{\mathbf{C}}_{\text{hi},k}(\bar{\mathbf{C}}_{\text{ih},k}\tilde{\mathbf{x}}_k + \bar{\mathbf{C}}_{\text{ih},k}\boldsymbol{x}_{\text{ref},k}) + \mathbf{N}\bar{\mathbf{C}}_{\text{hi},k}\hat{\mathbf{Z}}_k \\ &= \mathbf{M}\tilde{\mathbf{x}}_k + \mathbf{M}\boldsymbol{x}_{\text{ref},k} + \mathbf{N}\bar{\mathbf{C}}_{\text{hi},k}\hat{\mathbf{Z}}_k \end{aligned} \tag{38}$$

Equation (38) can now be applied to the feedback control law in the Hill frame

$$\begin{aligned} \boldsymbol{u}_{\text{h},k} &= -\mathbf{K}(\bar{\mathbf{x}}_k - \boldsymbol{x}_{\text{ref},k}) \\ &= (-\mathbf{KM})\tilde{\mathbf{x}}_k - (\mathbf{KN}\bar{\mathbf{C}}_{\text{hi},k})\hat{\mathbf{Z}}_k + \mathbf{K}(1 - \mathbf{M})\boldsymbol{x}_{\text{ref},k} \end{aligned} \tag{39}$$

The overall objective is to define the updated error term, $\tilde{\mathbf{x}}_{k+1}$, in terms of the states $\tilde{\mathbf{x}}_k$ and $\hat{\mathbf{Z}}_k$. From equation (34), we have

$$\tilde{\mathbf{x}}_{k+1} = \boldsymbol{x}_{k+1} - \boldsymbol{x}_{\text{ref},k+1} \tag{40}$$

Beginning with the reference trajectory term, we have

$$\boldsymbol{x}_{\text{ref},k+1} = \boldsymbol{\Phi}_\text{h}\boldsymbol{x}_{\text{ref},k} \tag{41}$$

Next, starting from the definition of the discrete LTV relative model in equation (31), the real relative state update can be solved using the control term from equation (39)

$$\begin{aligned} \boldsymbol{x}_{k+1} &= \boldsymbol{\Phi}_\text{h}\boldsymbol{x}_k + \mathbf{B}_\text{h}\boldsymbol{u}_{\text{h},k} \\ &= \boldsymbol{\Phi}_\text{h}(\boldsymbol{x}_k + \boldsymbol{x}_{\text{ref},k}) + \mathbf{B}_\text{h}[(\mathbf{KM})\tilde{\mathbf{x}}_k + (-\mathbf{KN}\bar{\mathbf{C}}_{\text{hi},k})\hat{\mathbf{Z}}_k \\ &\quad + \mathbf{K}(1 - \mathbf{M})\boldsymbol{x}_{\text{ref},k}] \\ &= (\boldsymbol{\Phi}_\text{h} - \mathbf{B}_\text{h}\mathbf{KM})\tilde{\mathbf{x}}_k + (-\mathbf{B}_\text{h}\mathbf{KN}\bar{\mathbf{C}}_{\text{hi},k})\hat{\mathbf{Z}}_k \\ &\quad + (\boldsymbol{\Phi}_\text{h} + \mathbf{B}_\text{h}\mathbf{K} - \mathbf{B}_\text{h}\mathbf{KM})\boldsymbol{x}_{\text{ref},k} \end{aligned} \tag{42}$$

Substituting equations (41) and (42) into equation (40), the state update for the tracking error term in the Hill

frame becomes

$$\tilde{\mathbf{x}}_{k+1} = (\mathbf{\Phi}_{\mathrm{h}} - \mathbf{B}_{\mathrm{h}}\mathbf{K}\mathbf{M})\tilde{\mathbf{x}}_k + (-\mathbf{B}_{\mathrm{h}}\mathbf{K}\mathbf{N}\bar{\mathbf{C}}_{\mathrm{hi},k})\hat{\mathbf{Z}}_k + \mathbf{B}_{\mathrm{h}}\mathbf{K}(1-\mathbf{M})\boldsymbol{x}_{\mathrm{ref},k} \tag{43}$$

where the bracketed expressions represent $\mathbf{\Phi}_{11,k}$, $\mathbf{\Phi}_{12,k}$, and $\mathbf{B}_1$, respectively, in the discrete LTV system of equation (35).

4.2 Development of the estimated relative state, $\hat{\mathbf{Z}}_{k+1}$

The next objective is to express the updated estimated relative state, $\hat{\mathbf{Z}}_{k+1}$, in terms of $\tilde{\mathbf{x}}_k$ and $\hat{\mathbf{Z}}_k$. From equation (34), the estimate at interval $k+1$ can be written as

$$\hat{\mathbf{Z}}_{k+1} = \hat{\mathbf{X}}_{\mathrm{d},k+1} - \hat{\mathbf{X}}_{\mathrm{c},k+1} \tag{44}$$

The state estimate of the deputy (i.e. position and velocity) at this step can be expanded into the general form of a linear observer

$$\hat{\mathbf{X}}_{\mathrm{d},k+1} = \mathbf{\Phi}_{\mathrm{i}}\hat{\mathbf{X}}_{\mathrm{d},k} + \mathbf{K}_{\mathrm{ss}}(\mathbf{Y}_{\mathrm{d},k} - \hat{\mathbf{Y}}_{\mathrm{d},k}) + \mathbf{B}_{\mathrm{i}}\boldsymbol{u}_{\mathrm{i},k} \tag{45}$$

where

$$\mathbf{Y}_{\mathrm{d},k} = \mathbf{H}\mathbf{X}_{\mathrm{d},k}, \quad \hat{\mathbf{Y}}_{\mathrm{d},k} = \mathbf{H}\hat{\mathbf{X}}_{\mathrm{d},k}, \quad \text{and} \quad \mathbf{H} = \begin{bmatrix} 1 & 0 & 0 & 0 & 0 & 0 \\ 0 & 1 & 0 & 0 & 0 & 0 \\ 0 & 0 & 1 & 0 & 0 & 0 \end{bmatrix}$$

The matrix $\boldsymbol{u}_{i,k}$ represents the control thrusts (there is no thrusting term in CanX-4&5's EKF (see equation (11)), since it would be difficult to combine a filter discretized at 5 s intervals with a pulse width modulated thrust discretized at 300 s. For the discrete LTV system, however, it is important to consider the control thrusts. Therefore the thrusts are discretized via a 5 s ZOH for their application to the discrete LTV system) from equation (39) rotated from the Hill frame into the GCI frame

$$\begin{aligned} \boldsymbol{u}_{i,k} &= \mathbf{C}_{\mathrm{ih},k}\boldsymbol{u}_{\mathrm{h},k} \\ &= \mathbf{C}_{\mathrm{ih},k}[(-\mathbf{K}\mathbf{M})\tilde{\mathbf{x}}_{\mathrm{k}} + (-\mathbf{K}\mathbf{N}\bar{\mathbf{C}}_{\mathrm{hi},k})\hat{\mathbf{Z}}_k \\ &\quad + (\mathbf{K} - \mathbf{K}\mathbf{M})\boldsymbol{x}_{\mathrm{ref},k}] \\ &= (-\mathbf{C}_{\mathrm{ih},k}\mathbf{K}\mathbf{M})\tilde{\mathbf{x}}_k + (-\mathbf{C}_{\mathrm{ih},k}\mathbf{K}\mathbf{N}\bar{\mathbf{C}}_{\mathrm{hi}})\hat{\mathbf{Z}}_k \\ &\quad + \mathbf{C}_{\mathrm{ih},k}\mathbf{K}(1-\mathbf{M})\boldsymbol{x}_{\mathrm{ref},k} \end{aligned} \tag{46}$$

Now equation (45) can be rewritten as

$$\begin{aligned} \hat{\mathbf{X}}_{\mathrm{d},k+1} &= \mathbf{\Phi}_i\mathbf{X}_{\mathrm{d},k} + \mathbf{K}_{ss}(\mathbf{H}\mathbf{X}_{\mathrm{d},k} - \mathbf{H}\hat{\mathbf{X}}_{\mathrm{d},k}) \\ &\quad + \mathbf{B}_i[(-\mathbf{C}_{\mathrm{ih},E}\mathbf{K}\mathbf{M})\tilde{\mathbf{x}}_k + (-\mathbf{C}_{\mathrm{ih},k}\mathbf{K}\mathbf{N}\bar{\mathbf{C}}_{\mathrm{hi}})\hat{\mathbf{Z}}_k \\ &\quad + \mathbf{C}_{\mathrm{ih},k}\mathbf{K}(1-\mathbf{M})\boldsymbol{x}_{\mathrm{ref},k}] \end{aligned} \tag{47}$$

The updated state estimate for the chief can be expanded from equation (44) as

$$\begin{aligned} \hat{\mathbf{X}}_{\mathrm{c},k+1} &= \mathbf{\Phi}_i\hat{\mathbf{X}}_{\mathrm{c},k} + \mathbf{K}_{ss}(\mathbf{Y}_{\mathrm{c},k} - \hat{\mathbf{Y}}_{\mathrm{c},k}) \\ &= \mathbf{\Phi}_i\hat{\mathbf{X}}_{\mathrm{c},k} + \mathbf{K}_{ss}(\mathbf{H}\mathbf{X}_{\mathrm{c},k} - \mathbf{H}\hat{\mathbf{X}}_{\mathrm{c},k}) \end{aligned} \tag{48}$$

Substituting equations (47) and (48) into equation (44), the update for the estimated relative state in the GCI frame can be reduced to

$$\begin{aligned} \hat{\mathbf{Z}}_{k+1} &= (\mathbf{K}_{ss}\mathbf{H}\bar{\mathbf{C}}_{\mathrm{ih},k} - \mathbf{B}_i\mathbf{C}_{\mathrm{ih},k}\mathbf{K}\mathbf{M})\tilde{\mathbf{x}}_k \\ &\quad + (\mathbf{\Phi}_i - \mathbf{K}_{ss}\mathbf{H} - \mathbf{B}_i\mathbf{C}_{\mathrm{ih},k}\mathbf{K}\mathbf{N}\bar{\mathbf{C}}_{\mathrm{hi},k})\hat{\mathbf{Z}}_k \\ &\quad + (\mathbf{K}_{ss}\mathbf{H}\bar{\mathbf{C}}_{\mathrm{ih},k} + \mathbf{B}_i\mathbf{C}_{\mathrm{ih},k}\mathbf{K}(1-\mathbf{M}))\boldsymbol{x}_{\mathrm{ref},k} \end{aligned} \tag{49}$$

Here the bracketed expressions represent $\mathbf{\Phi}_{21,k}$, $\mathbf{\Phi}_{22,k}$, and $\mathbf{B}_2$, respectively, in the discrete LTV system of equation (35). Now equations (43) and (49) can be substituted into equation (35), and the full discrete LTV system for CanX-4&5 becomes

$$\begin{aligned} \begin{bmatrix} \tilde{\mathbf{x}} \\ \hat{\mathbf{Z}} \end{bmatrix}_{k+1} &= \begin{bmatrix} \mathbf{\Phi}_{\mathrm{h}} - \mathbf{B}_{\mathrm{h}}\mathbf{K}\mathbf{M} & -\mathbf{B}_{\mathrm{h}}\mathbf{K}\mathbf{N}\bar{\mathbf{C}}_{\mathrm{hi},k} \\ \mathbf{K}_{ss}\mathbf{H}\bar{\mathbf{C}}_{\mathrm{ih},k} & \mathbf{\Phi}_i - \mathbf{K}_{ss}\mathbf{H} \\ -\mathbf{B}_i\mathbf{C}_{\mathrm{ih},k}\mathbf{K}\mathbf{M} & -\mathbf{B}_i\mathbf{C}_{\mathrm{ih},k}\mathbf{K}\mathbf{N}\bar{\mathbf{C}}_{\mathrm{hi},k} \end{bmatrix}_k \begin{bmatrix} \tilde{\mathbf{x}} \\ \hat{\mathbf{Z}} \end{bmatrix}_k \\ &\quad + \begin{bmatrix} \mathbf{B}_{\mathrm{h}}\mathbf{K}(1-\mathbf{M}) \\ \mathbf{K}_{ss}\mathbf{H}\bar{\mathbf{C}}_{\mathrm{ih},k} + \mathbf{B}_i\mathbf{C}_{\mathrm{ih},k}\mathbf{K}(1-\mathbf{M}) \end{bmatrix}_k \boldsymbol{x}_{\mathrm{ref},k} \end{aligned} \tag{50}$$

Since the state of the chief satellite changes at each time step, the values of $\bar{\mathbf{C}}_{\mathrm{ih},k}$, $\bar{\mathbf{C}}_{\mathrm{hi},k}$, and $\mathbf{C}_{ih,k}$, and thus the value of $\mathbf{\Phi}_k$, will also change throughout the course of an orbit. Although orbital perturbation forces will cause a slow regression of the chief's perigee from one orbit to the next, the change is small on the scale of the full orbit. Therefore, we can assume that the system is periodic and that $\mathbf{\Phi}_k = \mathbf{\Phi}_{k+N}$, where $T = N\Delta t$ is the orbital period. As such, we can employ discrete Floquet theory to determine the periodic stability of the system.

5 APPLICATION OF DISCRETE FLOQUET THEORY FOR STABILITY DETERMINATION

Given the discrete LTV system, $\mathbf{X}_{k+1} = \mathbf{\Phi}_k\mathbf{X}_k$, with N time steps in one period, the state transition matrix $\mathbf{\Phi}_k = \mathbf{\Phi}_{k+N}$ if the system is periodic. For one full orbit, we have

$$\mathbf{X}_N = \mathbf{\Phi}^*\mathbf{X}_0 \tag{51}$$

where

$$\mathbf{\Phi}^* = \prod_{k=1}^{N} \mathbf{\Phi}_k$$

According to discrete Floquet theory, the stability of the periodic system can be determined by the eigenvalues of $\mathbf{\Phi}^*$. For n states, the system is globally asymptotically stable if the eigenvalues satisfy $|\lambda_i\{\mathbf{\Phi}^*\}| < 1$ for $i = 1, \ldots, n$ [**15**].

6 STABILITY RESULTS

In the case of CanX-4&5, the matrix $\mathbf{\Phi}^*$ is determined by computing the cumulative product of $\mathbf{\Phi}_k$ from equation (50) at each time step k for one full orbital period. A circular, Sun-synchronous orbit was used to simulate the mission, with the orbital elements given in Table 1.

The chief has an orbital period of $\sim T = 5740$ s, which yields $N = 1148$ steps for a discretization time of 5 s.

6.1 ATO and PCO formations

With the discrete LTV model added to FIONA, a single orbit in each formation of the mission was individually simulated, the matrix $\mathbf{\Phi}^*$ calculated for each orbit, and the eigenvalues $\lambda_i\{\mathbf{\Phi}^*\}$ evaluated. Since the stability of the system is independent of the reference trajectory, each formation (ATO and PCO) yielded identical eigenvalues. As Table 2 indicates, the magnitude of each eigenvalue is less than unity, signifying that the discrete LTV system of equation (50) is stable.

The eigenvalues, however, depend on whether or not the gravity terms are included in the orbital dynamics of equation (25) (which affects $\mathbf{\Phi}_i$ in equation (50)). Table 2 compares the eigenvalues for the baseline case where the gravity terms are ignored in the orbital dynamics of equation (25) and the case where the gravity terms are included. While ignoring the gravity terms in the dynamics of equation (25) decreases the representative realism of the system and increases one eigenvalue predominantly, it ultimately does not jeopardize the stability of this system. The stability of the control system also depends explicitly on the level of control authority used to design the LQR gain. The gain matrix was designed with an input cost of $\mathbf{R} = \text{diag}\{1.2 \times 10^4, 1.2 \times 10^4, 1.2 \times 10^4\}$ and a state cost of $\mathbf{Q} = \text{diag}\{2.8 \times 10^{-5}, 2.8 \times 10^{-5}, 2.8 \times 10^{-5}, 0.78, 0.78, 0.78\}$.

To verify the stability of the system, the eigenvalues of $\mathbf{\Phi}^*$ were also computed for the second orbit (i.e. for the interval $t = T \rightarrow 2T$). They were found to exactly match the eigenvalues of $\mathbf{\Phi}^*$ computed over the interval $t = 0 \rightarrow T$, confirming a periodic, stable system. The stability of FIONA can be demonstrated via numerical simulation. In Fig. 3, the Cartesian tracking error of the deputy is displayed for 50 orbits in a 1000 m ATO formation and there is no evidence of error growth or divergence.

Table 1 Orbital elements for CanX-4&5 mission

Eccentricity	0
Right ascension	99.56°
Argument of perigee	0°
Altitude at perigee	550 km
Time of perigee passage	0 s
Inclination	97.6°

Table 2 Eigenvalues of the CanX-4&5 discrete LTV system for ATO and PCO formations

$\lvert\lambda_i\{\mathbf{\Phi}^*\}\rvert$ (no gravity terms)	$\lvert\lambda_i\{\mathbf{\Phi}^*\}\rvert$ (gravity incl.)
1.554×10^{-1}	1.166×10^{-2}
5.529×10^{-3}	1.166×10^{-2}
5.529×10^{-3}	1.241×10^{-2}
1.425×10^{-3}	8.339×10^{-4}
1.425×10^{-3}	8.339×10^{-4}
1.410×10^{-4}	1.174×10^{-5}
1.280×10^{-6}	1.302×10^{-6}
1.280×10^{-6}	6.762×10^{-7}
6.340×10^{-7}	6.762×10^{-7}
6.340×10^{-7}	6.658×10^{-7}
1.130×10^{-7}	6.658×10^{-7}
1.130×10^{-7}	4.371×10^{-7}

6.2 The quasi J_2-invariant formation

One of the principal directions of formation flying satellite research is the development of advantageous dynamics and control strategies that will minimize the amount of fuel required to maintain a formation of satellites with an acceptable accuracy. Following the primary mission, CanX-4&5 will test a set of trajectories designed to reduce the control effort necessary to maintain the formation. In reference [**10**],

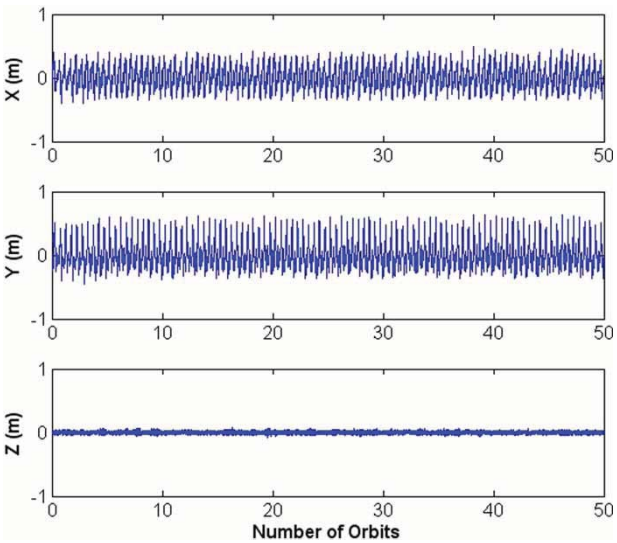

Fig. 3 Tracking error for 50 orbits in a 1000 m ATO formation

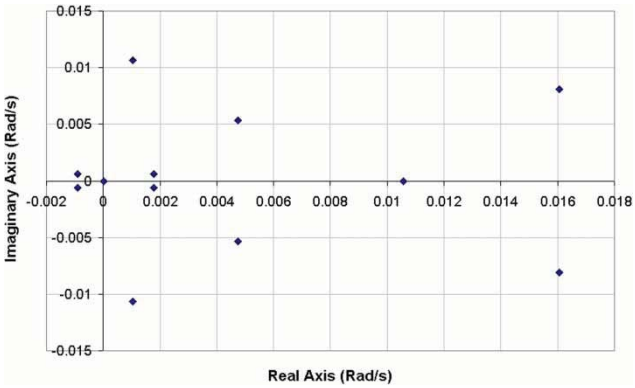

Fig. 4 Eigenvalues of the CanX-4&5 discrete LTV system for quasi J_2-invariant formations

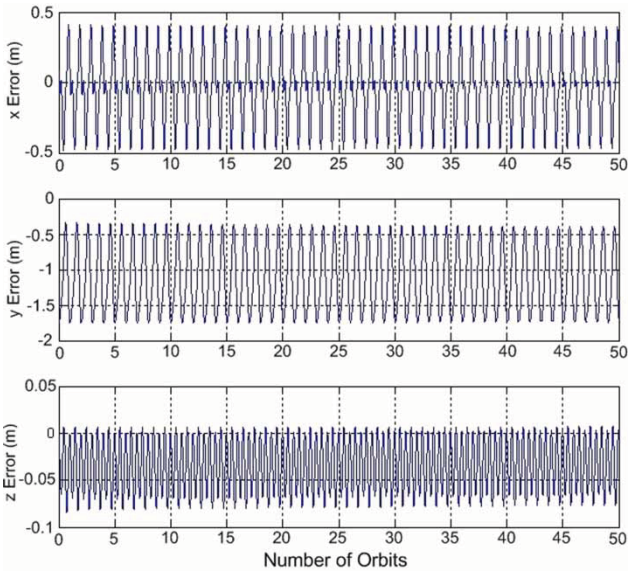

Fig. 5 Tracking error for 50 orbits in a quasi J_2-invariant formation

the authors developed these 'quasi J_2-invariant' trajectories using an iterative method to generate closed relative orbits that closely matched the natural relative dynamics of the satellites to help minimize fuel consumption. The technique relied on a shooting approach to the Newton method to determine a set of quasi-periodic (i.e. periodic over at least one orbit) initial conditions for the orbit [**16**]. To render the Newton method convergent, a low-authority linear state-feedback control law was introduced. Reference trajectories were generated by iteratively fitting a Fourier series to the actual perturbed motion of the deputy. This technique was successfully applied to the well-known J_2-invariant orbits [**17**] to produce trajectories that were quasi-periodic and highly robust to initial condition errors. With the development of the discrete LTV model, it is possible to apply Floquet theory to the quasi J_2-invariant orbit to determine the stability of CanX-4&5's controller while tracking this formation (although $\mathbf{\Phi}^*$ is independent of the reference trajectory, the quasi J_2-invariant trajectories require different initial conditions for the chief from the ATO and PCO trajectories and different $\mathbf{R}$ and $\mathbf{Q}$ values for the controller).

In keeping with the formation configuration used in reference [**10**], the chief was assigned the orbit given in Table 1 and the deputy was assigned the quasi J_2-invariant initial conditions from reference [**10**] with a relative satellite separation of 400 m. The matrix $\mathbf{\Phi}^*$ was computed over the course of one orbit in this formation, and the corresponding eigenvalues were computed. As illustrated in Fig. 4, all the eigenvalues are much less than unity, signifying that the CanX-4&5 control algorithm is stable while tracking quasi J_2-invariant orbits.

The stability of the system can again be demonstrated by running the numerical simulation of the CanX-4&5 mission over 50 orbits in the quasi J_2-invariant formation. Figure 5 shows the Cartesian tracking error in the Hill frame over that interval, and there is no evidence of either secular error growth or divergence.

As before, the stability of the algorithm depends on the level of control authority used to design the LQR gain. For the basic quasi J_2-invariant formation presented above, the input cost was $\mathbf{R} = \text{diag}\{8, 8, 8\}$ and the state cost was $\mathbf{Q} = \text{diag}\{1.2 \times 10^{-6}, 1.2 \times 10^{-6}, 1.2 \times 10^{-6}, 0.78, 0.78, 0.78\}$. This weak control authority is sufficient to maintain accurate periodicity for low fuel consumption, with $\Delta V = 0.007\,802$ m/s/orbit and a periodicity error $E_{10} = 0.008\,017$ m, where

$$E_N = \sqrt{\begin{matrix}[x(0) - x(NT)]^2 + [y(0) - y(NT)]^2 \\ +[z(0) - z(NT)]^2\end{matrix}} \tag{52}$$

and where N is the number of orbits over which the periodicity of the formation is tested (unlike ATO and PCO formations, where the emphasis is on precisely tracking pre-established reference trajectories, the focus of the quasi J_2-invariant orbits is to achieve maximally periodic motion from one orbit to the next for minimum ΔV. For this reason, our performance metric becomes the periodicity error, E_N rather than the tracking error $\tilde{\mathbf{x}}$). By reducing the control authority further while ensuring that the eigenvalues remain less than unity, it is possible to design a controller that minimizes fuel consumption and still maintains stability. Figure 6 shows the eigenvalues of $\mathbf{\Phi}^*$ when the control authority has been reduced to the stability limit, where $\mathbf{R} = \text{diag}\{1 \times 10^{10}, 1 \times 10^{10}, 1 \times 10^{10}\}$.

Propagated over 75 orbits, this solution has the performance metrics $\Delta V = 0.000\,485$ m/s/orbit and $E_{75} = 2.78$ m, an extremely low fuel requirement for moderate periodicity error. Figure 7 illustrates the

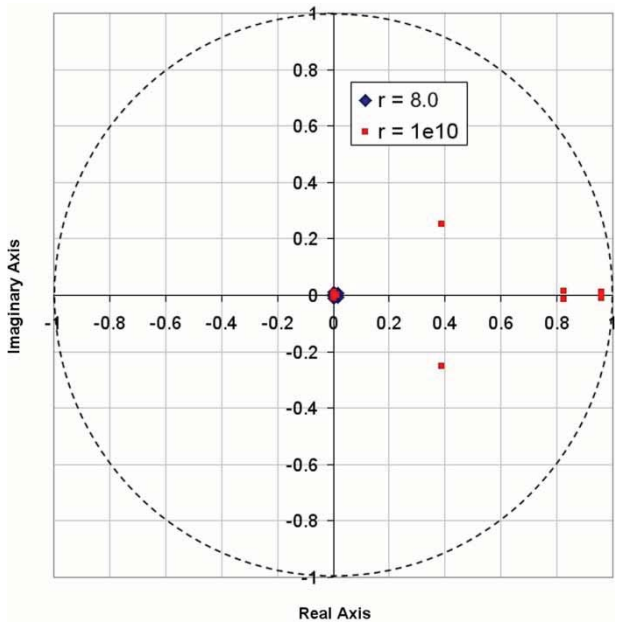

Fig. 6 Eigenvalues of Φ^* near the stability limit for quasi J_2 invariant formations

tracking error – used here to monitor periodic motion, but not to evaluate tracking performance – over the 75 orbits in the Hill frame. Since there is significant transient motion in the y-direction during the first orbit, the periodicity error E_N was taken from the beginning of the second orbit. While not exhibiting genuinely periodic motion between the initial and final orbits, the deputy nevertheless settles into a limit cycle after ∼50 orbits. This is indicative of a stable controller and a periodic orbit.

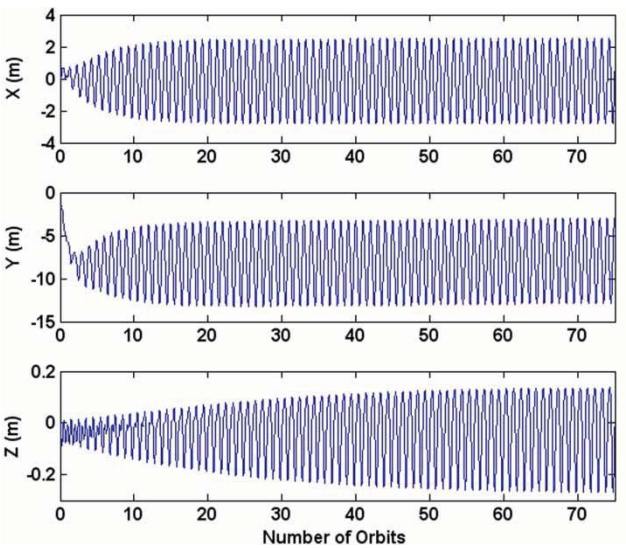

Fig. 7 Tracking error for 75 orbits in the quasi J_2-invariant orbit with $r = 1 \times 10^{10}$

7 CONCLUSIONS

The control algorithm for the CanX-4&5 formation flying nanosatellite mission was converted into a periodic LTV system to permit the stability of the algorithm to be analytically determined. The development of the discrete LTV system began with the linearization and discretization of the inertial orbital dynamics, the discretization of the relative HCW dynamics, and the conversion of the state-dependent EKF to a CGEKF. A suitable state for the discrete LTV system was selected, consisting of the relative error term in the Hill frame, $\tilde{\mathbf{x}}_k$, and the relative EKF estimate in the GCI reference frame, $\hat{\mathbf{Z}}_k$. A state transition matrix, $\mathbf{\Phi}_k$, was developed such that the discrete LTV model took the form $[\tilde{\mathbf{x}}^{\mathrm{T}}\ \hat{\mathbf{Z}}^{\mathrm{T}}]^{\mathrm{T}}_{k+1} = \mathbf{\Phi}_k[\tilde{\mathbf{x}}^{\mathrm{T}}\ \hat{\mathbf{Z}}^{\mathrm{T}}]^{\mathrm{T}}_k + [\mathbf{B}_1\ \mathbf{B}_2]^{\mathrm{T}}_k \boldsymbol{x}_{\mathrm{ref},k}$. Using discrete Floquet theory, the cumulative product of $\mathbf{\Phi}_k$ was found at each time step in one orbit and its eigenvalues were computed to determine the stability of the system. This analysis was applied to a numerical simulation of the ATO and PCO orbits of the primary mission of CanX-4&5. The absolute value of each eigenvalue was found to be less than unity, indicating a stable system. The stability of FIONA was also demonstrated numerically by observing the bounded tracking error over 50 orbits. The stability analysis was also applied to a quasi J_2-invariant orbit, a trajectory that is designed to minimize the amount of fuel required to maintain the formation of satellites. The control authority was reduced until it approached the stability limit of the controller and a minimum ΔV requirement of 0.000 485 m/s/orbit was found to guarantee stable performance for a quasi J_2-invariant orbit.

ACKNOWLEDGEMENTS

The authors would like to gratefully acknowledge the ongoing contributions of the CanX student team: Michael Greene, Guy de Carufel, Grant Bonin, Benoit Larouche, Mark Dwyer, Mohamed Ali, Amee Shah, Jonathan Gryzmisch, Chris Short, and Maria Short. In addition, the authors wish to thank the SFL staff for their support: Alex Beattie, Stuart Eagleson, Cordell Grant, Daniel Kekez, Stephen Mauthe, Freddy Pranajaya, Tarun Tuli, and Rob Zee.

REFERENCES

1 **Gill, E., D'Amico, S.,** and **Montenbruck, O.** Autonomous formation flying for the PRISMA mission. In Proceedings of the 16th AAS/AIAA Space Mechanics Meeting, Tampa, Florida, 2006.

2 **Borde, J., Teston, F., Santandrea, S.,** and **Boulade, S.** Feasibility of the proba-3 formation flying demonstration mission as a pair of microsats in GTO. In Proceedings of the 4S Symposium: Small Satellites, Systems and Services, La Rochelle, France, September 2004.

3 **de Ruiter, A.** A fault-tolerant magnetic spin stabilizing controller for the JC2Sat-FF mission. In Proceedings of the AIAA Guidance, Navigation and Control Conference and Exhibit, Hawaii, August 2008.

4 **Beugnon, C., Calvel, B., Boulade, S.,** and **Ankersen, F.** Design and modeling of the formation flying GNC system for the DARWIN interferometer. *Model. Syst. Eng. Astron.*, 2004, **5497**, 28–38.

5 **Hsiao, F.** and **Scheeres, D.** Design of spacecraft formation orbits relative to a stabilized trajectory. *J. Guid. Control Dyn.*, 2005, **28**(4), 782–794.

6 **Açikmeşe, B., Hadaegh F., Scharf, D.,** and **Ploen, S.** Formulation and analysis of stability for spacecraft formations. *IET Control Theory Appl.*, 2007, **1**(2), 461–474.

7 **Hu, Y.** and **Ng, A.** Robust control of spacecraft formation flying. *J. Aerosp. Eng.*, 2007, **20**(4), 209–214.

8 **Radice, G.** and **Biamonti, D.** Quasi optimal spacecraft formation maneuvering via lyapunov functions. *J. Aerosp. Eng. Sci. Appl.*, 2008, **1**(1), 18–24.

9 **Eyer, J., Damaren, C., Zee, R.,** and **Cannon, E.** A formation flying control algorithm for the CanX-4&5 low earth orbit nanosatellite mission. *Space Technol.*, 2007, **27**(4), 147–158.

10 **Eyer, J.** and **Damaren, C.** Quasi periodic relative trajectory generation for formation flying satellites. *J. Guid. Control Dyn.*, 2008 (in press).

11 **Leung, W.** and **Damaren, C. J.** A comparison of the pseudo-linear and extended Kalman filters for spacecraft attitude estimation. In Proceedings of the AIAA Guidance, Navigation, and Control Conference and Exhibit, Rhode Island, August 2004.

12 **Schaub, H.** and **Junkins, J. L.** *Analytical mechanics of space systems* 2003, pp. 593–602 (AIAA, Reston, Virginia, USA).

13 **de Ruiter, A., Lee, J., Kim, Y.,** and **Ng, A.** A computationally efficient near-optimal Kalman filter implementation for GPS-based spacecraft orbit and relative position and velocity determination, part 1: steady-state (submitted for publication).

14 **Ogata, K.** *Discrete-time control systems*, 2nd edition, 1995 (Prentice Hall, Englewood Cliffs, New Jersey).

15 **Park, S., Horowitz, R.,** and **Tan, C.** Digital implementation of adaptive control algorithms for mems gyroscopes. California PATH Research Report, UCB-ITS-PRR-2002-12, University of California, Berkeley, March 2002.

16 **Damaren, C. J.** Almost periodic relative orbits under J2 perturbations. *Proc. IMechE, Part G: J. Aerospace Engineering*, 2007, **221**(5), 767–774. DOI: 10.1243/09544100JAERO200.

17 **Schaub, H.** and **Alfriend, K. T.** J_2-invariant relative orbits for spacecraft formations. *Celest. Mech. Dyn. Astron.*, 2001, **79**(2), 77–95.

APPENDIX

Notation

$\boldsymbol{a}_{\text{thrust}}$	unit thrust vector
$\mathbf{A}_{\text{cd}}$	discretized orbital dynamics for the chief and deputy
$\mathbf{B}_{\text{h}}$, $\mathbf{B}_{\text{i}}$	discretized input matrix in the Hill and GCI reference frames
$\mathbf{C}_{\text{hi}}$, $\mathbf{C}_{\text{ih}}$	rotation matrices from GCI $\rightarrow$ Hill and from Hill $\rightarrow$ GCI
$\bar{\mathbf{C}}_{\text{hi}}$, $\bar{\mathbf{C}}_{\text{ih}}$	rotation matrices for full states from GCI $\rightarrow$ Hill and from Hill $\rightarrow$ GCI
C_j	constants of integration for HCW equations ($j = 1, 2, 3$)
E_N	periodicity error over N orbits
EKF	extended Kalman filter
GCI	geocentric inertial reference frame
$\boldsymbol{h}_k$	estimated position at step k
$\boldsymbol{H}_{\text{c}}$	angular momentum of the chief
$\mathbf{H}_k$	local observation matrix for the EKF
J_2	second zonal gravitational harmonic, $1.082\,626\,9 \times 10^{-3}$
$\mathbf{K}$	LQR controller gain matrix
$\mathbf{K}_k$	Kalman gain matrix for the EKF
$\mathbf{K}_{\text{ss}}$	steady state Kalman gain for the CGEKF
$\mathbf{M}, \mathbf{N}$	selection matrices for position and velocity, respectively
$\mathbf{P}_k^-$, $\mathbf{P}_k^+$	EKF covariance matrix just before/after the measurements
$\mathbf{Q}, \mathbf{R}$	state cost and input cost matrices for the LQR controller
$\mathbf{Q}_k$, $\mathbf{R}_k$	process and noise covariance matrices for the EKF
$\mathbf{R}_{\text{c}}$, $\mathbf{R}_{\text{d}}$	GCI states for the chief and deputy
R_{e}	equatorial radius of the Earth
t_{on}	thruster on time
$\boldsymbol{u}_{\text{h}}$, $\boldsymbol{u}_i$	control thrusts in the Hill and GCI reference frames
U_{max}	constant maximum thrust per unit mass
$\boldsymbol{x}$	relative state of the deputy in the Hill frame
$\boldsymbol{x}_{\text{ref}}$	reference trajectory in the Hill frame
$\tilde{\mathbf{x}}$	tracking error in the Hill frame
$\bar{\mathbf{x}}$	the 'real' relative state used in the feedback controller
$\mathbf{X}$	inertial state of both chief and deputy in the GCI reference frame
$\hat{\mathbf{X}}$	estimated state of both satellites in the GCI frame
$\mathbf{Y}_{\text{d}}$, $\hat{\mathbf{Y}}_{\text{d}}$	position and estimated position for the EKF
$\mathbf{Z}, \hat{\mathbf{Z}}$	relative state and estimated relative state of the deputy in the GCI
α	initial formation phase angle
θ	true anomaly
λ_n	eigenvalues of $\boldsymbol{\Phi}^*$ for n states
μ	Earth's gravitational constant
ω	mean orbital motion
$\boldsymbol{\Phi}_k$	state transition matrix
$\boldsymbol{\Phi}^*$	cumulative product of $\boldsymbol{\Phi}_k$ over one complete orbit